metals

MDPI

Article

Heterogeneous Deformation-Induced Strengthening Achieves the Synergistic Enhancement of Strength and Ductility in Mg–Sc Alloys

Wei Zhao [1], Mengyu Zhang [1], Ruxia Liu [1,2] and Jian Zhang [1,*]

[1] State Key Lab of Advanced Technology for Materials Synthesis and Processing, Wuhan University of Technology, Wuhan 430070, China
[2] School of Materials Science and Engineering, Wuhan University of Technology, Wuhan 430070, China
* Correspondence: zhangjian178@whut.edu.cn

Abstract: Magnesium alloys are essential lightweight materials for engineering applications. However, conventional single-phase hexagonal close-packed (HCP) magnesium alloys exhibit poor cold workability and insufficient strength at room temperature, which limits their engineering applications. Compared to HCP structures with limited slip systems at room temperature, body-centered cubic (BCC) structures possess 12 independent slip systems, enabling better plasticity. Therefore, Mg–Sc alloys with a dual-phase structure (HCP + BCC) exhibit superior plasticity compared to single-phase HCP magnesium alloys. In this study, the deformation behavior of dual-phase Mg-19.2 at.% Sc alloy was investigated, revealing its deformation characteristics and multiscale strengthening mechanisms. Experimental findings indicate that with the rise in annealing temperature, the volume fraction of the α phase progressively declines, while that of the β phase expands. Moreover, the grain size of the α phase first grows and then reduces, whereas the β phase grain size consistently enlarges. When the annealing temperature reaches 600 °C, the alloy exhibits an optimal strength–ductility combination, with an ultimate tensile strength of 329 MPa and an elongation of 20.5%. At this condition, the α phase volume fraction is 20%, while the β phase volume fraction is 80%, with corresponding grain sizes of 5.9 μm and 30.1 μm, respectively. Microstructural analysis indicates that the plastic incompatibility between the α and β phases induces significant heterogeneous deformation-induced (HDI) strengthening. Moreover, the unique bimodal grain size distribution, where the α phase grains are significantly smaller than the β phase grains, enhances the "hard phase harder, soft phase softer" heterogeneous structural effect, further amplifying the HDI strengthening contribution. This study provides new theoretical insights into multiphase interface engineering for designing high-performance dual-phase magnesium alloys.

Keywords: Mg–Sc alloy; annealing; heterostructure; HDI strengthening

check for updates

Academic Editors: Andrey Belyakov and Dmytro Orlov

Received: 6 March 2025
Revised: 6 April 2025
Accepted: 16 April 2025
Published: 18 April 2025

Citation: Zhao, W.; Zhang, M.; Liu, R.; Zhang, J. Heterogeneous Deformation-Induced Strengthening Achieves the Synergistic Enhancement of Strength and Ductility in Mg–Sc Alloys. *Metals* **2025**, *15*, 457. https://doi.org/10.3390/met15040457

Copyright: © 2025 by the authors. Licensee MDPI, Basel, Switzerland. This article is an open access article distributed under the terms and conditions of the Creative Commons Attribution (CC BY) license (https://creativecommons.org/licenses/by/4.0/).

1. Introduction

Magnesium alloys, recognized for their low density, superior mechanical properties, and outstanding electrical and thermal conductivities, hold significant potential for applications in the aerospace, defense, and military sectors [1–3]. However, due to their hexagonal close-packed (hcp) structure with strong anisotropy, magnesium alloys exhibit poor cold workability, which significantly limits their applications [4,5]. As a result, many studies have attempted to improve the workability of magnesium alloys by transforming the crystal structure from hcp to body-centered cubic (bcc), which is more isotropic. The first

magnesium alloy found to possess a bcc structure was the Mg–Li alloy. Research shows that the crystal structure of Mg–Li alloys is highly dependent on lithium content [6,7]. When the Li concentration is below 5.7%, Li fully dissolves into the Mg matrix, resulting in a pure α-Mg phase. When the Li concentration ranges from 5.7% to 10.3%, the alloy displays a two-phase structure of α-Mg and β-Li. When the Li concentration exceeds 10.3%, all Mg atoms dissolve into the Li matrix, forming a single body-centered cubic (bcc) β-Li phase. Although bcc-structured Mg–Li alloys exhibit excellent ductility, their low strength, poor creep resistance and corrosion resistance, and unstable natural aging behavior limit their broader application [8,9]. In 2016, Ogawa et al. [10] discovered that a β-type Mg-20.5 at.% Sc alloy exhibits a shape memory effect in space, with its parent phase being body-centered cubic (bcc). This is currently the only magnesium alloy aside from Mg–Li that can form both hcp and bcc crystal structures, providing a new direction for the development of bcc-structured magnesium alloys. Therefore, breaking through conventional magnesium alloy systems and developing Mg–Sc alloys with excellent strength and ductility at room temperature holds significant potential for expanding the application of magnesium alloys across various fields.

A review of existing studies on Mg–Sc alloys reveals that, through proper control of heat treatment processes, their microstructure—including phase composition, phase morphology, grain size, and crystallographic texture—can be tailored to influence mechanical properties [11–15]. Ogawa et al. [11] produced Mg-20 at.% Sc alloys with single α phase, dual (α + β) phase, and β phase microstructures by adjusting heat treatment parameters. Moreover, the grain sizes of dual-phase Mg-20 at.% Sc alloys vary with the proportion of each phase. When the volume fraction of the α phase is 34%, the combination of isotropic deformation of the β phase, refined grain size of the matrix phase, and a low c/a ratio of the α phase contributes to a synergy of high strength and large elongation, achieving a tensile strength of 312 MPa and an elongation of 28.8%. In addition, Ando et al. [12,13] found that the needle-like α phase precipitated during low-temperature aging of β-Mg-16.8 at.% Sc and dual-phase Mg-20.5 at.% Sc alloys can significantly enhance their tensile strength. Therefore, investigating the evolution of dual-phase microstructures in Mg–Sc alloys during heat treatment and their influence on mechanical properties is of great practical importance for optimizing heat treatment processes.

In recent years, rational design and the introduction of heterogeneous structures have become effective strategies for overcoming the strength–ductility tradeoff in metallic materials [16–18]. In heterogeneous structure materials, soft regions (coarse grains/soft phases) and hard regions (fine grains/hard phases) form during processing. These heterogeneous zones lead to non-uniform deformation, giving rise to hetero-deformation-induced (HDI) strengthening effects while maintaining good ductility. For example, Ren et al. [19] constructed a dual-phase heterogeneous lamella (DPHL) structure consisting of FCC and B2 phases in cold-rolled and annealed AlCoCrFeNi2.1 (at.%) EHEAs, achieving ultra-high yield strength (~1500 MPa) and excellent elongation (~16%). Wang et al. [20] developed a heterogeneous microstructure consisting of alternating coarse-grained (CG) and fine-grained (FG) layers in a Mg–9Al–1Zn–1Sn alloy by using simple rolling and carefully controlled annealing. This resulted in a yield strength of 251 MPa, an ultimate tensile strength of 393 MPa, and a ductility of 23%. For Mg–Sc alloys, naturally existing dual-phase components offer an intrinsic advantage for optimizing their mechanical properties through heterogeneous structure design. Therefore, controlling the microstructure of Mg–Sc alloys via heat treatment to achieve a desirable strength–ductility balance is key to developing high-performance Mg–Sc alloys.

In this research, Mg-19.2 at.% Sc alloy was subjected to annealing at various temperatures of 500, 550, and 600 °C for 30 min to examine the impact of annealing temperature

on the alloy's microstructure and mechanical properties. The findings indicate that the microstructures of the Mg-19.2 at.% Sc alloy annealed at 500, 550, and 600 °C are all composed of α and β phases, with the proportion of the α phase diminishing as the annealing temperature rises. When the alloy is heat-treated at 600 °C, it exhibits a heterogeneous structure characterized by a bimodal grain size distribution, resulting in excellent comprehensive mechanical properties, with a tensile yield strength of 329 MPa and an elongation of 20.5%.

2. Experimental Methods

High-purity magnesium (99.99%) and scandium were used as raw materials to prepare Mg–Sc alloys in a vacuum induction melting furnace under an argon protective atmosphere, provided by the Hunan Rare Earth Metal Materials Research Institute (Changsha, China). The nominal composition of the alloy was Mg-19.2 at.% Sc (Mg-30.5 wt.% Sc). To achieve a uniform composition, the alloy ingots were melted again four times and then gradually cooled within the furnace. The resulting ingots had a thickness of 15 mm (as shown in Figure 1) and were hot-rolled at 650 °C to a thickness of 3 mm. Subsequently, the sheets underwent repeated cycles of cold rolling and annealing at 550 °C for 10 min, until the final thickness reached approximately 2 mm. The rolling direction during both hot and cold rolling was maintained parallel. The thickness reduction per pass during hot rolling and cold rolling was kept below 10% and 2%, respectively. The processed thin sheets were cut into several pieces, which were then annealed at 500, 550, and 600 °C for 30 min, followed by water quenching. The complete experimental process flow is illustrated in Figure 2.

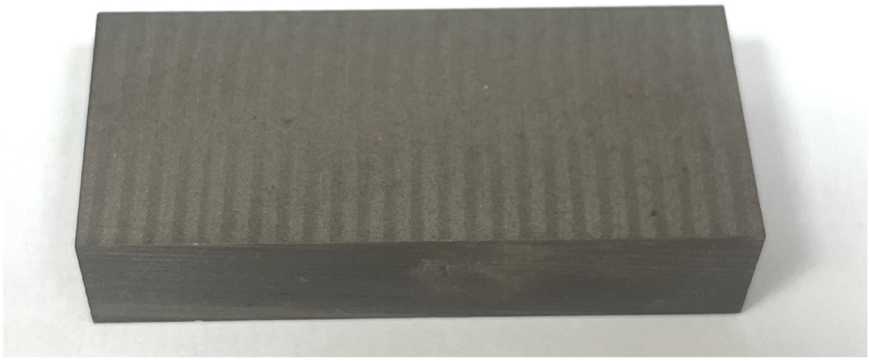

Figure 1. As-cast ingot of the Mg-19.2 at.% Sc alloy.

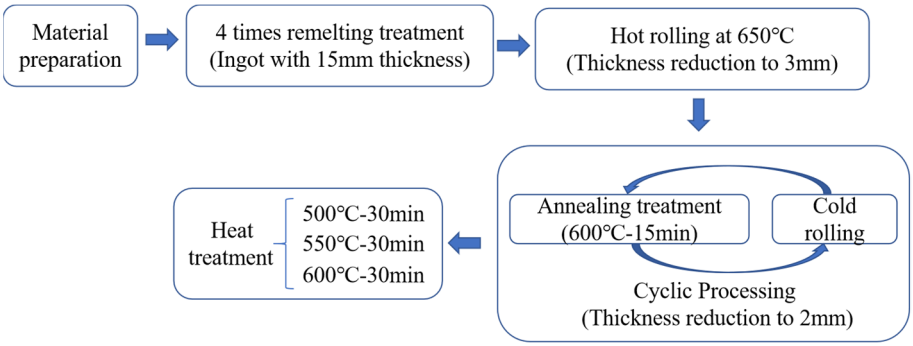

Figure 2. Schematic diagram of the experimental process.

Phase composition analysis of samples annealed at different temperatures was conducted using an Empyrean-type X-ray diffraction (XRD) instrument from PANalytical B.V., Eindhoven, The Netherlands. The measurements employed a Cu target radiation source, with a scanning range of 20–80°, a scanning rate of 2°/min, and operating conditions of 50 kV accelerating voltage and 40 mA current. The microstructure of the samples was

examined using field-emission scanning electron microscopy (FE-SEM), which included backscattered electron (BSE) imaging and electron backscatter diffraction (EBSD) analysis. For SEM–BSE imaging, mechanical polishing using SiC paper and diamond suspension was sufficient to obtain a mirror-like surface. However, for EBSD analysis, additional surface preparation with Ar ion polishing was carried out to remove the damaged surface layer after mechanical polishing.

Tensile samples were fabricated in accordance with the national standard GB/T 228.1-2021 [21], utilizing wire electrical discharge machining (EDM) to cut specimens with a gauge length of 10 mm and a gauge width of 3 mm from the rolled plates. Tensile experiments were performed using an Instron-5966 universal testing system from Norwood, MA, USA at ambient temperature, with an initial strain rate of 10^{-3} s^{-1}. To ensure data reliability, each heat treatment condition was tested three times under the same parameters. Fractography of the fractured tensile specimens was conducted using the secondary electron (SE) imaging mode of an electron microscope.

3. Results

Figure 3 displays the XRD patterns of the Mg-19.2 at.% Sc alloys treated at various temperatures for 30 min. As depicted in Figure 3, the XRD pattern of the specimen annealed at 500 °C shows prominent diffraction peaks, attributed to the α phase, along with relatively faint peaks of the β phase, suggesting that the microstructure predominantly consists of the α phase with a minor amount of the β phase. With an increase in the annealing temperature, the relative intensity of the diffraction peaks reveals a gradual reduction in the α phase content, accompanied by a corresponding rise in the β phase content. When the annealing temperature reaches 600 °C, the XRD pattern shows dominant peaks of the β phase, accompanied by weak peaks of the α phase, suggesting that the microstructure is predominantly β phase with minor α phase. The XRD results show that as the annealing temperature rises, the intensity of the β phase diffraction peaks becomes more pronounced, suggesting a phase change from the α phase to the β phase in the alloy.

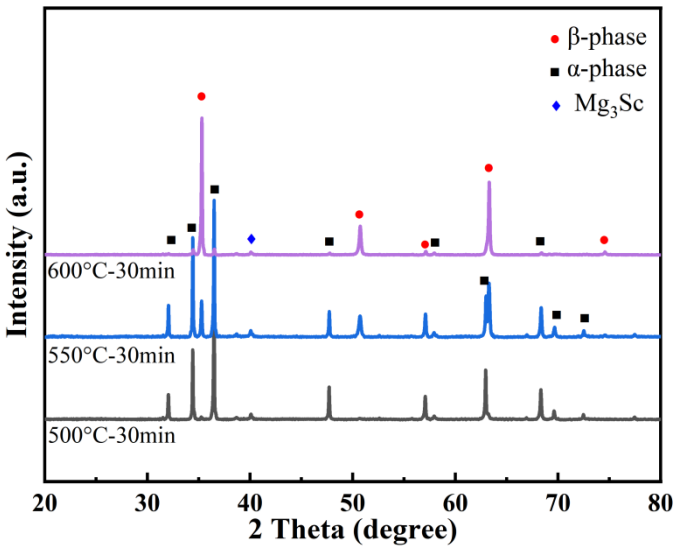

Figure 3. XRD patterns of the Mg-19.2 at.% Sc samples annealed at 500, 550, and 600 °C for 30 min.

Figure 4 shows the engineering stress–strain curves of the Mg-19.2 at.% Sc alloy under room-temperature tensile testing, and the corresponding mechanical properties are summarized in Table 1. According to the data in the table, the alloy annealed at 500 °C exhibits a tensile strength of 350 MPa and an elongation of 12.7%. At this temperature, the alloy demonstrates relatively high tensile strength but limited ductility. However, with

increasing annealing temperature, the alloy shows a slight reduction in strength but a significant improvement in ductility, indicating enhanced plastic deformation capacity. When the annealing temperature reaches 600 °C, the alloy exhibits a tensile strength of 329 MPa and an excellent elongation of 20.5%. Compared with the alloy annealed at 500 °C, the elongation increases by 61.4%, while the tensile strength decreases by only 6%, which contradicts the conventional strength–ductility trade-off theory in alloys. Therefore, it is necessary to further investigate the underlying microstructural mechanisms responsible for the improved ductility at 600 °C annealing without a noticeable reduction in yield strength.

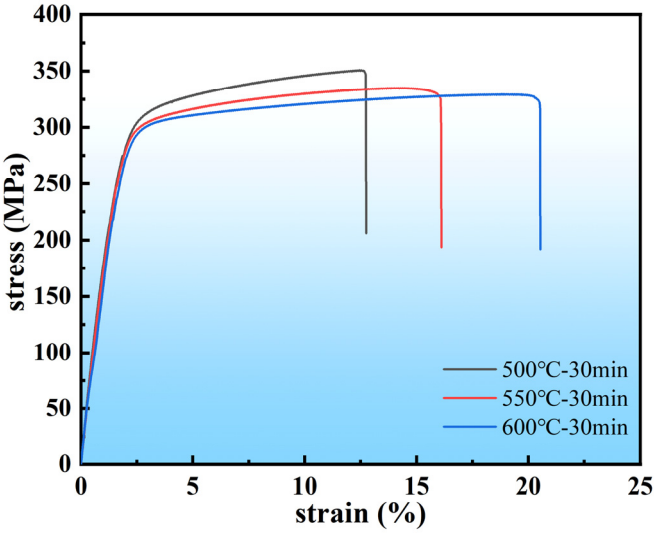

Figure 4. Room temperature tensile engineering stress–strain curves of the Mg-19.2 at.% Sc samples annealed at 500, 550, and 600 °C for 30 min.

Table 1. Yield strength (YS), ultimate tensile strength (UTS), and elongation (EL) of the Mg-19.2 at.% Sc samples annealed at 500, 550, and 600 °C for 30 min.

Annealing Temperature (°C)	YS (MPa)	UTS (MPa)	EL (%)
500	308.6	350	12.7
550	289.3	335	16.1
600	280.1	329	20.5

To investigate the microstructural evolution during annealing, backscattered electron (BSE) imaging was performed on samples annealed at 500, 550, and 600 °C for 30 min, as shown in Figure 5a–f. From the images, it is clearly observed that the microstructure of the Mg-19.2 at.% Sc alloy prior to heat treatment consists of two distinct regions: dark areas and light gray areas. In BSE imaging, contrast arises from differences in atomic number within different regions of the microstructure. Regions with higher atomic numbers produce stronger backscattered electron signals, resulting in brighter contrast in the image [22]. Since scandium (Sc) has a higher atomic number than magnesium (Mg), the dark regions in the BSE images correspond to the α phase, while the light gray regions correspond to the β phase. Figure 5a shows a predominantly single α phase microstructure after annealing at 500 °C, and the magnified image in Figure 5d reveals a small amount of β phase within the α matrix. Figures 5b and 5c display dual-phase (α + β) microstructures for samples annealed at 550 °C and 600 °C, respectively; however, the volume fraction of the α phase at 600 °C is significantly lower than that at 550 °C. As the annealing temperature increases, the volume fraction of the β phase increases, which is consistent with the XRD results.

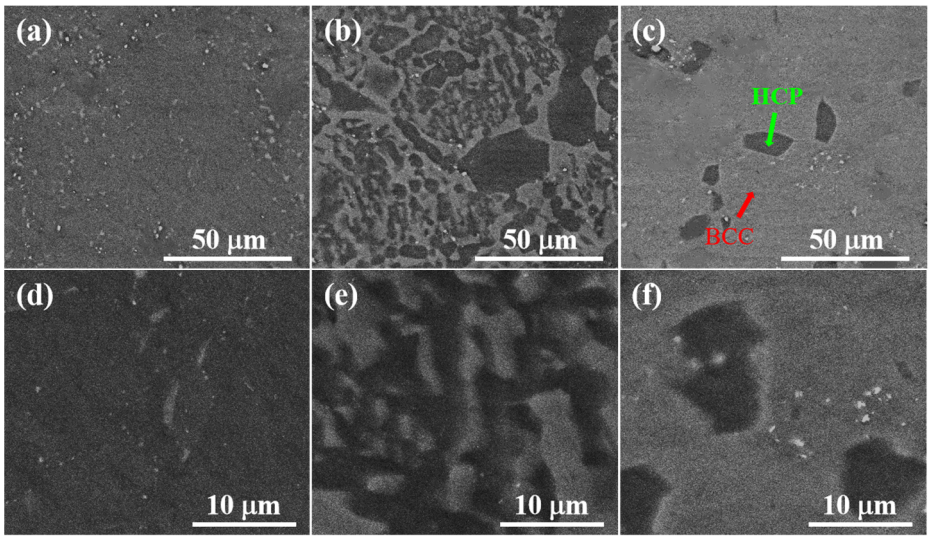

Figure 5. BSE images of the Mg-19.2 at.% Sc samples annealed at different temperatures: (**a**,**d**) 500 °C; (**b**,**e**) 550 °C; (**c**,**f**) 600 °C.

Fractographic analysis is one of the most important qualitative methods for investigating the fracture behavior of magnesium alloys. The fracture surfaces of materials exhibit distinct morphologies depending on the fracture mode. In general, magnesium alloys fracture either in a brittle or in a ductile manner. To reveal the damage and fracture mechanisms, Figure 6 presents the typical fracture morphologies of the Mg-19.2 at.% Sc alloys annealed at different temperatures. The fracture surface of the alloy annealed at 500 °C is mainly characterized by intergranular and quasi-cleavage fracture features, indicative of a brittle fracture mode. For the alloy annealed at 550 °C, the quasi-cleavage region decreases, and ductile dimples begin to appear, suggesting a mixed brittle–ductile fracture mode. When the annealing temperature reaches 600 °C, the fracture surface is predominantly composed of ductile dimples, with an increased number of dimples, smaller sizes, and greater depths, indicating a clear ductile fracture mode. This observation is consistent with the enhanced plastic deformation and the highest elongation measured in the mechanical testing.

Figure 7 presents the inverse pole figure (IPF) maps of the alloy, illustrating the texture orientations of the α and β grains. For the sample annealed at 500 °C, distinct differences in the texture orientations of the α and β grains are observed. The texture proportion of β grains along the <111> direction is significantly higher than that along other directions, while the α grains exhibit a more diverse range of texture orientations. Further analysis of the texture orientation changes of α and β grains at different temperatures reveals that with increasing temperature, the texture proportion of β grains along the <111> direction gradually decreases, while the texture proportion along the <001> direction gradually increases. In contrast, the texture proportion of α grains along the <-12-10> direction significantly increases. Based on quantitative calculations, the strength of the sample with the <111> texture at 500 °C is approximately 7.06, while the strength of the <-12-10> texture is approximately 1.66. At 600 °C, the strength of the sample with the <001> texture is approximately 7.41, and the strength of the <-12-10> texture is approximately 1.03. A comparison reveals that the texture strength variation in the sample with the most dominant texture at different annealing temperatures is not significant. Overall, the Mg-19.2 at.% Sc alloy still exhibits a multi-orientation texture distribution at different temperatures, consistent with previous studies [23,24], indicating that its texture has a limited impact on the mechanical properties.

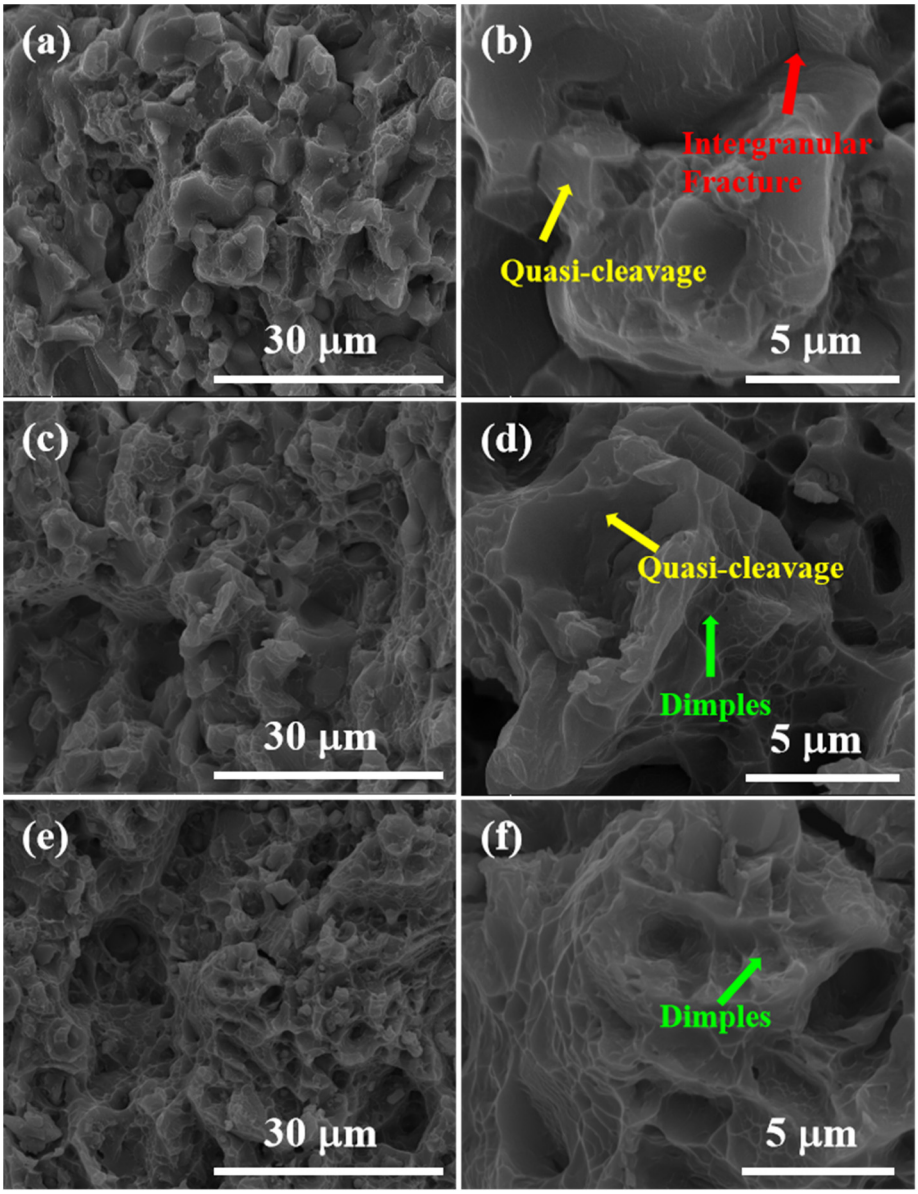

Figure 6. Fractography of the Mg-19.2 at.% Sc samples annealed at different temperatures after the tensile fracture: (**a**,**b**) 500 °C; (**c**,**d**) 550 °C; (**e**,**f**) 600 °C.

To further elucidate the microscopic mechanisms responsible for the high strength and plasticity of the alloy annealed at 600 °C, EBSD analysis was conducted to investigate the evolution of the α and β phases and their corresponding grain sizes, as shown in Figure 8. The green regions represent the α phase, while the red regions represent the β phase. As the annealing temperature increases, the volume fraction of the β phase increases, which is consistent with the XRD and SEM–BSE results. As shown in Table 1, the volume fractions of the β phase in the samples annealed at 500, 550, and 600 °C are 5.2%, 34.7%, and 80%, respectively. In contrast to the α phase, which has a hexagonal close-packed (HCP) structure and a limited number of slip systems at room temperature, the β phase, with a body-centered cubic (BCC) arrangement, has 12 distinct slip systems. Given that the β phase volume fraction is greatest in the sample treated at 600 °C, this condition demonstrates the highest ductility. Moreover, after annealing at 500 and 550 °C, the mean grain size of the alloy stayed below 10 μm. However, following annealing at 600 °C, the mean grain size of the α phase was 5.9 μm, while the β phase grain size substantially grew to 30.1 μm, as presented in Table 2. Notably, the grain size distribution of the α and β phases in the 600 °C

annealed sample exhibits a bimodal structure, where smaller α phase grains are uniformly distributed around the larger β phase grain boundaries, forming a "soft + hard" dual-phase heterogeneous structure. The plastic incompatibility between the α and β phases induces significant heterogeneous deformation-induced (HDI) strengthening. Furthermore, the unique bimodal grain size distribution, in which the α phase grains are significantly smaller than the β phase grains, enhances the heterogeneous structural effect of "hard phase harder, soft phase softer", further amplifying the HDI-strengthening contribution.

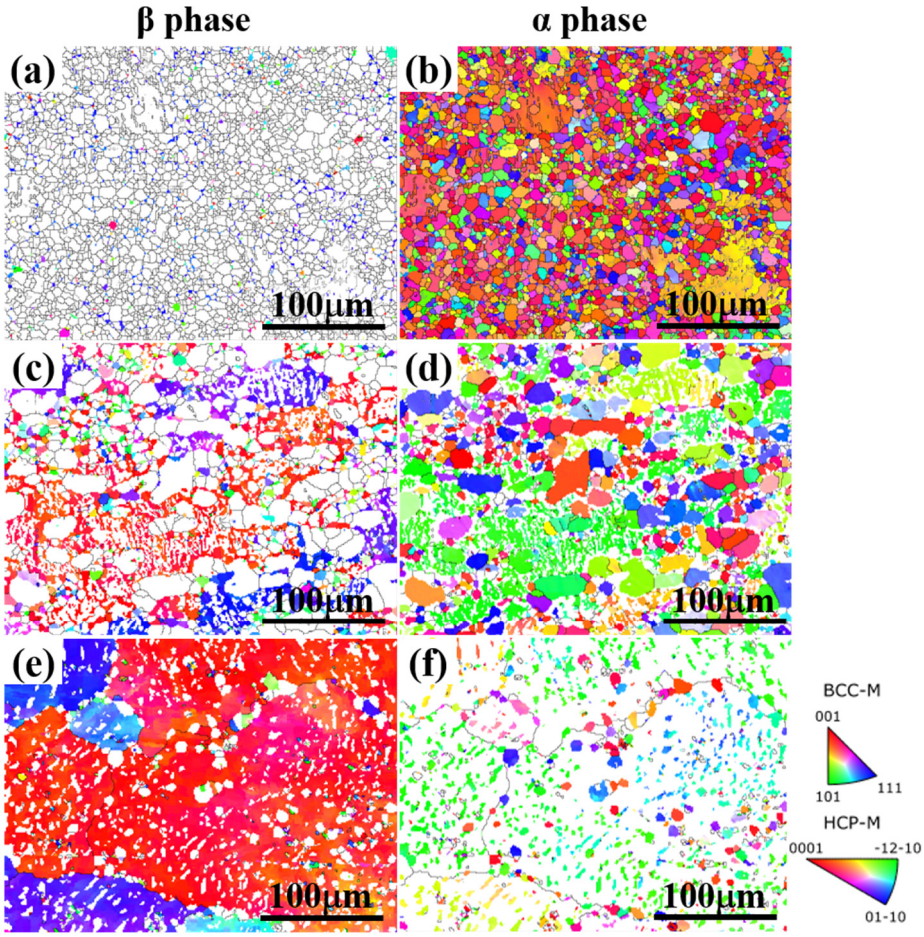

Figure 7. IPF map of the Mg-19.2 at.% Sc alloy annealed at different temperatures: (**a**,**b**) 500 °C; (**c**,**d**) 550 °C; (**e**,**f**) 600 °C.

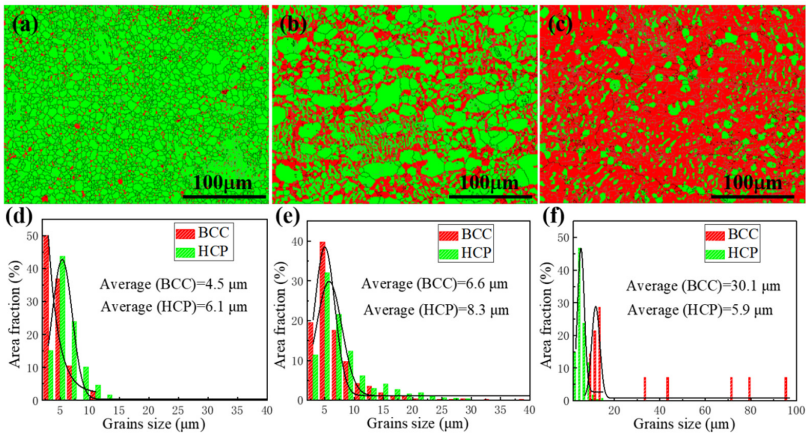

Figure 8. Phase maps, statistical histograms, and distribution curves of the Mg-19.2 at.% Sc samples annealed at different temperatures: (**a**,**d**) 500 °C; (**b**,**e**) 550 °C; (**c**,**f**) 600 °C.

Table 2. The volume fraction and grain size of the α/β phase in the Mg-19.2 at.% Sc samples annealed at different temperatures.

Annealing Temperature (°C)	Volume Fraction of α Phase (%)	Grain Size of α Phase (μm)	Volume Fraction of β Phase (%)	Grain Size of β Phase (μm)
500	94.8	6.1	5.2	4.5
550	65.3	8.3	34.7	6.6
600	20	5.9	80	30.1

The specific strengthening mechanism is as follows: During tensile deformation, dislocation slip is first activated in the soft BCC phase, while the hard HCP phase remains elastic. Due to the mechanical differences between these two regions, plastic incompatibility arises between the soft and hard zones, where the plastic deformation of the soft zone is constrained by the hard zone. Although the soft zone undergoes plastic deformation and accommodates more strain, the interface between the soft and hard zones must maintain continuity. As a result, a deformation gradient forms in the softer zone near the interface to maintain strain compatibility, requiring the accumulation of geometrically necessary dislocations (GNDs) to facilitate coordinated deformation. When the hard region begins to plastically deform, GNDs primarily accumulate in the soft region near the heterogeneous interface. Since these dislocations cannot propagate across the interface, they generate back stress in the soft region, counteracting the applied stress and making the soft region appear stronger. Simultaneously, forward stress is generated in the hard region, making it appear weaker. The coupling of these effects manifests as macroscopic HDI strengthening, providing additional strength and strain-hardening capability. HDI strain hardening helps prevent premature necking during deformation, thereby improving ductility and enhancing the strength–ductility synergy of the heterogeneous structure [25,26]. Consequently, the HDI strengthening effect is the key strengthening mechanism of the Mg-19.2 at.% Sc alloy after annealing.

To enhance the strength and ductility of Mg–Sc alloys, this study primarily achieves optimization by regulating the phase fraction and grain size. However, what has garnered more attention recently is the presence of two types of martensitic transformations in Mg–Sc alloys. Mg alloys with 20.5 at.% Sc and lower Sc content exhibit a body-centered cubic (BCC)-to-orthorhombic martensitic transformation during low-temperature plastic deformation, demonstrating shape memory characteristics [27,28]. Additionally, in β-Mg-22.55 at.% Sc and β-Mg-35 wt.% Sc alloys, another stress-induced martensitic transformation occurs at room temperature, specifically a BCC-to-hexagonal close-packed (HCP) transformation, which endows the alloy with a pronounced transformation-induced plasticity (TRIP) effect [15,29]. The TRIP effect is a strengthening mechanism that utilizes austenitic transformation to achieve a balance between strength and ductility. This mechanism has been widely applied in the design and development of high-manganese steels, titanium alloys, and high-entropy alloys with excellent mechanical properties. Therefore, the rational tuning of metastable β phase stability and microstructure to realize transformation-induced plasticity is expected to be a key research focus for enhancing the strength and ductility of Mg–Sc alloys in the future.

4. Conclusions

This study investigates the effect of annealing temperature on the microstructure and mechanical properties of the Mg-19.2 at.% Sc alloy, aiming to explore the microstructural evolution and strengthening mechanisms of the α+β dual-phase structure. The results show that as the annealing temperature increases, the ductility of the alloy gradually improves, while the yield strength slightly decreases. The alloy annealed at 600 °C exhibits

the best combination of yield strength (280.1 MPa) and ductility (20.5%). Microstructural observations reveal that with increasing annealing temperature, the volume fraction of the β phase increases, while that of the α phase decreases. The β phase, with a body-centered cubic (BCC) structure, provides more favorable slip systems during tensile deformation, thereby enhancing the ductility of the alloy. Furthermore, EBSD analysis shows that when the annealing temperature increases from 500 °C to 600 °C, the grain size of the β phase grows to 30 μm, while the α phase grain size decreases to a minimum of 5.9 μm, forming a "soft + hard" bimodal heterogeneous structure. The Mg-19.2 at.% Sc alloy annealed at 600 °C achieves an excellent balance between yield strength and ductility due to hetero-deformation-induced (HDI) strengthening arising from the heterogeneous microstructure composed of coarse-grained BCC phase and fine-grained HCP phase.

Author Contributions: Conceptualization, J.Z.; methodology, W.Z., M.Z. and R.L.; software, W.Z. and M.Z.; validation, W.Z., M.Z. and R.L.; formal analysis, W.Z., M.Z. and R.L.; investigation, W.Z. and M.Z.; resources, J.Z.; data curation, W.Z., M.Z. and R.L.; writing—original draft preparation, W.Z.; writing—review and editing, W.Z. and M.Z. All authors have read and agreed to the published version of the manuscript.

Funding: This work was financially supported by the National Natural Science Foundation of China (grant No. 52401136), the Natural Science Foundation of Jiangsu Province (BK20220549).

Data Availability Statement: The original contributions presented in this study are included in the article. Further inquiries can be directed to the corresponding author.

Conflicts of Interest: The authors declare no conflict of interest.

References

1. Xing, F.; Li, S.; Yin, D.; Xie, J.; Rommens, P.M.; Xiang, Z.; Liu, M.; Ritz, U. Recent progress in Mg-based alloys as a novel bioabsorbable biomaterials for orthopedic applications. *J. Magnes. Alloys* **2022**, *10*, 1428–1456. [CrossRef]
2. Kim, B.; Hong, C.H.; Kim, J.C.; Lee, S.-Y.; Baek, S.-M.; Jeong, H.Y.; Park, S.S. Factors affecting the grain refinement of extruded Mg-6Zn-0.5Zr alloy by Ca addition. *Scr. Mater.* **2020**, *187*, 24–29. [CrossRef]
3. Zhao, D.; Chen, X.; Ci, W.; Liu, C.; Pan, F. Effect of Al element on microstructure, mechanical properties and damping capacity of LPSO-containing Mg-Y-Zn-Li alloy. *Mater. Charact.* **2024**, *207*, 113542. [CrossRef]
4. Liu, R.X.; Zhao, W.; Wu, G.L.; Wang, S.; Zhang, J.; Xiao, Y.; Mao, X. A high-performance TRIP Mg-Sc-Zn alloy enhanced by fine grain strengthening and nano-precipitate strengthening. *J. Mater. Res. Technol.* **2024**, *33*, 3874–3881. [CrossRef]
5. Ovri, H.; Markmann, J.; Barthel, J.; Kruth, M.; Dieringa, H.; Lilleodden, E.T. Mechanistic origin of the enhanced strength and ductility in Mg-rare earth alloys. *Acta Mater.* **2023**, *224*, 118550. [CrossRef]
6. Tian, G.Y.; Wang, J.S.; Wang, S.; Xue, C.; Yang, X.; Su, H.; Yang, Z.; Yan, C.; Liu, X.; Dou, R. Achieving ultra-high stiffness by solidifying and precipitating micro-compounds in HCP/BCC dual matrix of a new Mg-Li alloy. *J. Alloys Compd.* **2023**, *964*, 171324. [CrossRef]
7. Wang, J.H.; Sun, D.P.; Wu, R.Z.; Du, C.; Yang, Z.; Zhang, J.; Hou, L. A good balance between mechanical properties and electromagnetic shielding effectiveness in Mg-9Li-3Al-1Zn alloy. *Mater. Charact.* **2022**, *188*, 111888. [CrossRef]
8. Jiang, B.; Zhang, C.H.; Wang, T.; Qu, Z.; Wu, R.; Zhang, M. Creep behaviors of Mg-5Li-3Al-(0, 1)Ca alloys. *Mater. Des.* **2012**, *34*, 863–866. [CrossRef]
9. Li, C.Q.; Xu, D.K.; Zhang, Z.R.; Han, E. Influence of the lithium content on the negative difference effect of Mg-Li alloys. *J. Mater. Sci. Technol.* **2020**, *57*, 138–145. [CrossRef]
10. Ogawa, Y.; Ando, D.; Sutou, Y.; Koike, J. A lightweight shape-memory magnesium alloy. *Science* **2016**, *353*, 368–370. [CrossRef]
11. Ogawa, Y.; Ando, D.; Sutou, Y.; Yoshimi, K.; Koike, J. Determination of α/β phase boundaries and mechanical characterization of Mg-Sc binary alloys. *Mater. Sci. Eng. A* **2016**, *670*, 335–341. [CrossRef]
12. Ando, D.; Ogawa, Y.; Suzuki, T.; Sutou, Y.; Koike, J. Age-hardening effect by phase transformation of high Sc containing Mg alloy. *Mater. Lett.* **2015**, *161*, 5–8. [CrossRef]
13. Ogawa, Y.; Ando, D.; Sutou, Y.; Koike, J. Aging Effect of Mg-Sc Alloy with α+β Two-Phase Microstructure. *Mater. Trans.* **2016**, *57*, 1119–1123. [CrossRef]
14. Ogawa, Y.; Singh, A.; Somekawa, H. Activation of non-basal <c+a> slip incoarse-grained Mg-Sc alloy. *Scr. Mater.* **2022**, *218*, 114830.

15. Xu, C.; Wang, J.F.; Wang, C.; Wang, W.; Sun, Y.; Guan, S.; Zhang, T. Martensitic transformation behavior during tensile testing at room temperature in β-type Mg-35 wt%Sc alloy. *Mater. Sci. Eng. A* **2023**, *865*, 144602. [CrossRef]
16. Li, Z.M.; Pradeep, K.G.; Deng, Y.; Raabe, D.; Tasan, C.C. Metastable high-entropy dual-phase alloys overcome the strength-ductility trade-off. *Nature* **2016**, *534*, 227–230. [CrossRef]
17. Zhu, Y.T.; Wu, X.L. Perspective on hetero-deformation induced (HDI) hardening and back stress. *Mater. Res. Lett.* **2019**, *7*, 393. [CrossRef]
18. Wu, X.L.; Yang, M.X.; Yuan, F.P.; Wu, G.; Wei, Y.; Huang, X.; Zhu, Y. Heterogeneous lamella structure unites ultrafine-grain strength with coarse-grain ductility. *Proc. Natl. Acad. Sci. USA* **2015**, *112*, 14501–14505. [CrossRef] [PubMed]
19. Ren, J.; Zhang, Y.; Zhao, D.; Chen, Y.; Guan, S.; Liu, Y.; Liu, L.; Peng, S.; Kong, F.; Poplawsky, J.D.; et al. Strong yet ductile nanolamellar high-entropy alloys by additive manufacturing. *Nature* **2022**, *608*, 62–68. [CrossRef]
20. Wang, H.; Zhang, D.T.; Qiu, C.; Zhang, W.; Chen, D. Achieving superior strength-ductility synergy in a heterostructured magnesium alloy via low-temperature extrusion and low-temperature annealing. *J. Mater. Sci. Technol.* **2023**, *163*, 32–44. [CrossRef]
21. *GB/T 228.1-2021*; Metallic Materials—Tensile Testing—Part 1: Method of Test at Room Temperature. China Standard Publishing House: Beijing, China, 2021.
22. Zhu, H.G.; Du, Y.L.; Zhao, J. *Modern Analytical Techniques for Materials*; National Defense Industry Press: Beijing, China, 2012.
23. Yamagishi, K.; Ando, D.; Sutou, Y.; Ogawa, Y. Texture formation through thermomechanical treatment and its effect on superelasticity in Mg-Sc shape memory alloy. *Mater. Trans.* **2020**, *61*, 2270–2275. [CrossRef]
24. Ogawa, Y.; Ando, D.; Sutou, Y.; Koike, J. Texture randomization of hexagonal close packed phase through hexagonal close packed/body centered cubic phase transformation in Mg-Sc alloy. *Scr. Mater.* **2017**, *128*, 27–31. [CrossRef]
25. Romero-Resendiz, L.; El-Tahawy, M.; Zhang, T.; Rossi, M.C.; Marulanda-Cardona, D.M.; Yang, T.; Amigó-Borrás, V.; Huang, Y.; Mirzadeh, H.; Beyerlein, I.J.; et al. Heterostructured stainless steel: Properties, current trends, and future perspectives. *Mater. Sci. Eng. R Rep.* **2022**, *150*, 100691. [CrossRef]
26. Lu, L.; Zhao, H.Z. Research Progress on Strengthening and Toughening Mechanisms of Heterogeneous Nanostructured Metals. *Acta Metall. Sin.* **2022**, *58*, 1360–1370.
27. Yamagishi, K.; Ogawa, Y.; Ando, D.; Sutou, Y.; Koike, J. Room temperature superelasticity in a lightweight shape memory Mg alloy. *Scr. Mater.* **2019**, *168*, 114–118. [CrossRef]
28. Tripathi, S.; Vishnu, K.G.; Titus, M.S.; Strachan, A. Tunability of martensitic transformation in Mg-Sc shape memory alloys: A DFT study. *Acta Mater.* **2020**, *189*, 1–9. [CrossRef]
29. Yamagishi, K.; Ogawa, Y.; Ando, D.; Sutou, Y. Adjustable room temperature deformation behavior of Mg-Sc alloy: From superelasticity to slip deformation via TRIP effect. *J. Alloys Compd.* **2023**, *931*, 167507. [CrossRef]

Disclaimer/Publisher's Note: The statements, opinions and data contained in all publications are solely those of the individual author(s) and contributor(s) and not of MDPI and/or the editor(s). MDPI and/or the editor(s) disclaim responsibility for any injury to people or property resulting from any ideas, methods, instructions or products referred to in the content.